Faraday Discuss., 1996, **105**, 337–354

Electronic structure, reactivity and solid-state chemistry of $La_{2-x}Sr_xNi_{1-y}Fe_yO_{4+\delta}$

Julian F. Howlett,[a] Wendy R. Flavell,[a,*] Andrew G. Thomas,[a] Jane Hollingworth,[a] Samantha Warren,[a] Zulkifli Hashim,[a] Michael Mian,[a] Steven Squire,[a] Hamid R. Aghabozorg,[a] Md. Moinuddin Sarker,[b] Paul L. Wincott,[c] David Teehan,[d] Stuart Downes,[d] Daniel S-L. Law[d] and Frederick E. Hancock[e]

[a] *Department of Physics, UMIST, P.O. Box 88, Manchester UK M60 1QD*
[b] *Department of Chemistry, UMIST, P.O. Box 88, Manchester UK M60 1QD*
[c] *Department of Chemistry/IRCSS, University of Manchester UK M13 9PL*
[d] *CLRC Daresbury Laboratory, Daresbury, Warrington, Cheshire UK WA4 4AD*
[e] *ICI Katalco R, T & E, P.O. Box 1, Billingham, Cleveland UK TS23 1LB*

Ceramic samples of $La_{2-x}Sr_xNi_{1-y}Fe_yO_{4+\delta}$, designed to model the ICI Hydecat catalyst, have been prepared *via* precipitation followed by high temperature annealing. The samples are characterized by X-ray diffraction, EDAX and atomic absorption spectrometry. The small changes in electronic structure as a function of x and y have been probed using photoemission. This reveals a progressive shift of the valence-band edge towards the Fermi level as a function of Sr-doping level, consistent with the approach to a metal to non-metal transition. Resonant photoemission at the Fe and Ni 3p thresholds is used to identify the transition metal contributions to the valence band density of states, and confirms a valence state of $\geqslant 3.0$ for Fe. High resolution ESCA is used to quantify the surface composition of the samples, revealing Sr segregation consistent with that found in related perovskites and layered perovskites. Adsorption of CO onto the surfaces of these materials is seen to give rise to the ready production of a carbonate species. Water adsorption studies, which test the potential stability of the materials for possible applications in aqueous solution, are also presented.

The electronic structure of complex transition metal oxides is of considerable interest, as the properties of these oxides can be tailored to specific applications by subtle changes in chemical doping. This allows the electronic conduction of the materials to be tuned from insulating to metallic and even superconducting. In addition, it is possible to stabilize certain ions in unusual valence states, leading to potential applications in oxidation catalysis. Modulation of the formal valency of the transition metal ion in these systems is achieved by doping at a counter-cation site.

Synchrotron-excited resonant photoemission is exceptionally powerful in revealing the atomic character of these states.[1] Here we apply the technique to a complex mixed transition metal–rare earth oxide system, $La_{2-x}Sr_xNi_{1-y}Fe_yO_{4+\delta}$. $La_{2-x}Sr_xNiO_{4+\delta}$ is the nickel analogue of the cuprate superconductor $La_{2-x}Sr_xCuO_{4+\delta}$. In common with this material, the formal transition metal valency can be raised above 2.0 by replacement of the trivalent La by divalent Sr, and the material also undergoes a non-metal to metal transition as x increases. In contrast with the cuprate, which becomes metallic for small values of x, the metallic phase in the nickelate is not achieved until x reaches at least 0.8,[2] at which point the majority of the Ni is in the Ni^{III} oxidation state. There have been very few studies of iron doping in this material, but Mössbauer studies suggest that Fe

can be maintained in the Fe^{IV} state in this material.[2] Thus in common with the superconducting cuprates, in this lattice, the transition metal ions appear to be stabilized in unusually high oxidation states, and these valencies can be controlled by the amount of Sr doping.

Our interest in this system stems from its potential use as a model to understand the behaviour of unusually high oxidation states for Ni and Fe in the ICI Katalco Hydecat aqueous hypochlorite decomposition catalyst. The addition of quite low levels of Fe to this catalyst results in anomalous enhancements in the catalytic activity of the nickel oxide based material. A mechanism has recently been proposed for the action of this catalyst, involving a rate-limiting interconversion of Ni^{II} to Ni^{III} during the catalytic cycle. Addition of Fe to the catalyst is thought to enhance Ni^{II}–Ni^{III} charge transfer through strong Fe–O–Ni interactions.[3] Here we study the changes in electronic structure of $La_{2-x}Sr_xNi_{1-y}Fe_yO_{4+\delta}$ as a function of both x and y, concentrating particularly on the character of the states close to the Fermi energy, E_F. As this is essentially equivalent to the chemical potential of the system, this gives us an insight into which states will be most easily involved in the catalytic redox cycle. Control of x allows us to vary the proportion of Ni^{III} present in the sample, while variation of y probes the influence of Fe on the Ni density of states (DOS) close to the Fermi energy.

One measurement has probed the Ni contribution to the valence band DOS function in the $y = 0$ material $La_{2-x}Sr_xNiO_4$,[4] using Ni $3p \rightarrow 3d$ resonant photoemission. Here, we use this resonance to study the Ni DOS in Fe co-doped materials, and also the corresponding Fe resonance to provide complementary information about the Fe valence band DOS. In addition, we study the effect of Sr doping on the valence band density of states in Fe doped and non-Fe containing samples.

We have also tested the oxidizing power and atmospheric/aqueous stability of the surfaces by adsorption of small probe molecules. Water adsorption under controlled conditions probes the initial stages of any surface degradation that might occur, *e.g.*, in the use of these materials in aqueous solution. These studies reveal that the reactivity of the surfaces to water is affected quite strongly by Sr doping. The longer term effects of degradation are probed by high resolution ESCA studies, which reveal Sr segregation to the surface, influencing the reactivity of the samples to atmospheric gases.

Experimental

$La_{2-x}Sr_xNi_{1-y}Fe_yO_{4+\delta}$ was produced by a coprecipitation route. Stoichiometric amounts of $LaCl_3 \cdot 7H_2O$, $Sr(NO_3)_2$, $NiCl_2 \cdot 6H_2O$ and $Fe(NO_3)_3 \cdot 9H_2O$ were dissolved in distilled water. The solution pH was adjusted to nine by addition of saturated Na_2CO_3 solution, and the resulting precipitate was filtered, washed and dried overnight at 120 °C. The glassy material was then ground and annealed at 897 °C for 10 h, before being reground and annealed at 1200 °C for 48 h. After a further regrinding, the material was annealed under oxygen for 20 h at 1170 °C.

The samples were characterized by X-ray diffraction (XRD), energy dispersive X-ray analysis (EDAX) and atomic absorption spectrometry (AAS). XRD was carried out using a Scintag XDS2000 automated powder diffractometer and monochromated Cu-Kα radiation. EDAX investigations were carried out in order to check the bulk composition of the samples synthesized, using a Phillips SEM 505 microscope with a 9100/60 system attachment for EDAX. AAS measurements were additionally carried out in order to quantify low doping levels. These used a Thermo Jarrell Ash Video 22E atomic absorption spectrometer.

Resonant photoemission measurements were carried out at the Synchrotron Radiation Source, CLRC Daresbury Laboratory. These measurements used the toroidal grating monochromator ($15 \leqslant h\nu \leqslant 90$ eV) on Station 6.2, with a Phi double-pass CMA. The position of the Fermi edge was determined by reference to the Mo sample holder.

For introduction into UHV, the powder samples were pressed into pellets, and these were reannealed under conditions identical to those used for the final stage of the synthesis, giving mechanical strength to the pellets. Sections of these were mounted onto an Mo sample plate using silver-loaded UHV-compatible epoxy resin. The surfaces of the materials to be studied were cleaned for UHV measurements by scraping using a diamond file *in vacuo* at 5×10^{-11}–10^{-10} mbar. Sample cleanliness was monitored using the valence band photoemission in the range 5–15 eV binding energy. The characteristic adsorption features that arise in the valence band photoemission due to surface contamination were established in a series of experiments involving the adsorption of small probe molecules normally present in the residual vacuum, such as CO and H_2O. Dosing was achieved using pure CO (Messer-Griesheim, 99.997%) or doubly-distilled water, which was thoroughly freeze-degassed before use. These were admitted to the vacuum chamber *via* a leak valve, with the exposure in langmuirs (1 L = 10^{-6} Torr s) estimated from the chamber ion gauge. The samples were initially cooled to around 125 K before dosing, and then warmed to room temperature. Spectra were recorded at intervals during this process.

High resolution ESCA studies were carried out using the Scienta ESCA 300 instrument at the RUSTI facility, CLRC Daresbury Laboratory. The Scienta instrument has a rotating anode Al-Kα X-ray source which is monochromated using seven double-focusing 3 inch diameter quartz crystals. It is fitted with a 300 mm mean radius hemispherical electrostatic analyser. In our work, spectra were obtained at 150 eV pass energy and 0.5 mm slit width, where the overall (source + analyser) resolution is of the order of 0.35 eV. As-presented samples were studied, with the aim of assessing the extent of reaction of the oxides with atmospheric gases.

Results and Discussion

Bulk characterization

XRD from $La_{2-x}Sr_xNi_{1-y}Fe_yO_{4+\delta}$ ($x = 0$–1, $y = 0$–0.2) showed the samples to be highly crystalline and essentially single phase, although for some compositions a small number of additional peaks were visible just above the background noise level. This suggests the presence of a small amount ($\leqslant 2\%$) of an unidentified second phase. EDAX and AAS results were consistent with the bulk nominal compositions.

Synchrotron radiation photoemission measurements

Valence band energy distribution curves (EDCs). Fig. 1 and 2 show the valence band spectra of $La_{2-x}Sr_xNi_{1-y}Fe_yO_{4+\delta}$ for samples containing no Fe ($y = 0$, Fig. 1), and for samples containing Fe ($y = 0.2$, Fig. 2). The valence band spectrum shows some similarities to that of NiO. The feature in the range 1–8 eV binding energy is predicted, by band structure calculations for NiO, to be of mixed O 2p–Ni 3d character.[5] The feature at around 10 eV binding energy is, in part, contaminant related; our adsorption measurements indicate that this feature grows in intensity with CO dosing, leading to the formation of a surface carbonate-like feature (see below). However, this region of the spectrum also includes a contribution from a valence band satellite feature, as observed in NiO,[6] and is discussed further below. Features in the range 18–24 eV binding energy are due to the low lying La 5p and Sr 4p levels; the latter increase in intensity with increasing Sr doping level.

Doping with Sr (whilst maintaining a constant oxygen content) increases the transition metal ion valencies, and corresponds to effective hole doping (as for the related cuprate $La_{2-x}Sr_xCuO_4$). As has been noted for a number of related complex transition metal systems,[7–9] the effect of this is often to move the position of the Fermi energy

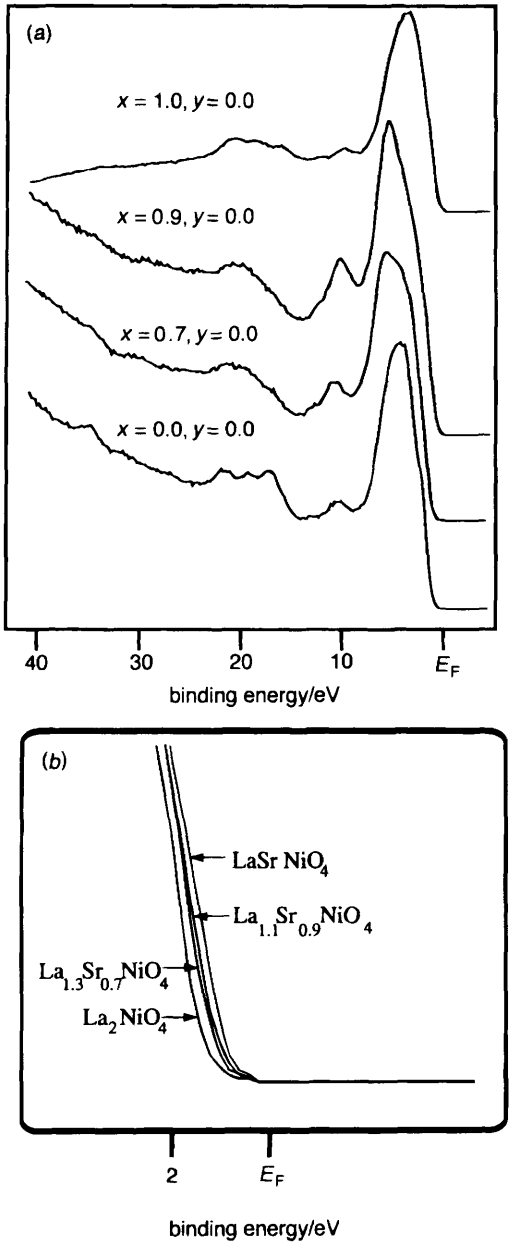

Fig. 1 (*a*) EDCs showing the valence band and satellite regions of a scraped ceramic sample of $La_{2-x}Sr_xNiO_{4+\delta}$ at 75 eV photon energy for varying Sr doping levels. (*b*) An enlargement of the valence band edge region showing the decrease in binding energy of the valence band edge as x increases.

within the gap closer to the valence band edge. Fig. 1 and 2 illustrate the movement of the valence band edge on Sr doping [this is enlarged in Fig. 1(*b*) and 2(*b*)]. For samples having $y = 0$ (*i.e.*, no Fe), the valence band edge moves towards E_F as a function of Sr doping, showing a total shift between $x = 0$ and $x = 1.1$ of around 0.5 eV, consistent

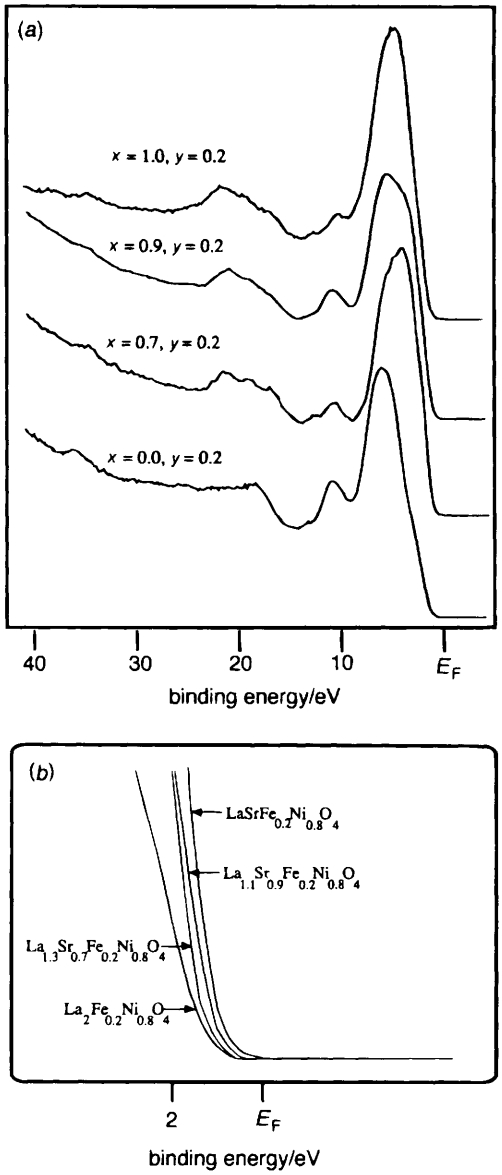

Fig. 2 (*a*) EDCs showing the valence band and satellite regions of a scraped ceramic sample of $La_{2-x}Sr_xNi_{1-y}Fe_yO_{4+\delta}$ at 75 eV photon energy for varying Sr doping levels. (*b*) An enlargement of the valence band edge region showing the decrease in binding energy of the valence band edge as x increases.

with the results of Eisaki *et al.*[4] For samples containing appreciable amounts of Fe (*e.g.*, $y = 0.2$, Fig. 2), a similar effect is observed, suggesting the approach to a metal to non-metal transition, but in this case a larger shift, of up to around 1 eV is seen on increasing x [Fig. 2(*b*)]. A distinct Fermi cut-off indicating metallic behaviour is not observed up to $x = 1.1$ for either Fe-doped or non-Fe containing samples. This indicates that the metal to non-metal transition has not been reached. The Sr doping level at which the metal to non-metal transition occurs in $La_{2-x}Sr_xNiO_{4+\delta}$ has not been accurately established.

Our results suggest that semiconducting behaviour persists above the level of $x \approx 0.8$ suggested by Takagi *et al.*[10] The upper limit for synthesis of solid solution samples in this system has very recently been identified as $x \approx 1.6$.[11] However, our attempts to synthesize samples with Sr content higher than $x = 1.1$ only resulted in materials that were extremely unstable to degradation, and did not retain their integrity sufficiently long to allow transfer into the UHV chamber. Nevertheless, it is clear that the doped nickelate behaves very differently from the corresponding superconducting cuprate, $La_{2-x}Sr_xCuO_4$, which becomes metallic for Sr contents as low as $x \approx 0.15$. This has been attributed to stronger electron–phonon coupling in the nickelate.[12]

Resonant photoemission. Resonant photoemission can also be used to probe the transition metal valency contribution to the valence band DOS, as shown in Fig. 3 and 4, which show EDC and constant initial state (CIS) mode data for $La_{2-x}Sr_xNi_{1-y}Fe_yO_{4+\delta}$. Fig. 3 shows valence band spectra for a sample of $La_2NiO_{4+\delta}$ recorded on resonance ($h\nu = 67$ eV) and off-resonance ($h\nu = 63$ eV) at the Ni 3p → 3d threshold. The difference spectrum (67–63 eV) is similar to that of Eisaki *et al.*[4] for this material, showing a shift in overall intensity to the satellite region at resonance. The observed resonance is quite weak, but it is nevertheless seen clearly in the CIS data of Fig. 4. Data are recorded at the valence band edge (1.2 eV binding energy), the valence band intensity maximum (4.3 eV binding energy) and the satellite feature (9.2 eV binding energy). The CIS spectra show a small anti-resonance at the valence band edge, and a resonance at the satellite feature. This resonance behaviour is also observed for Sr- and

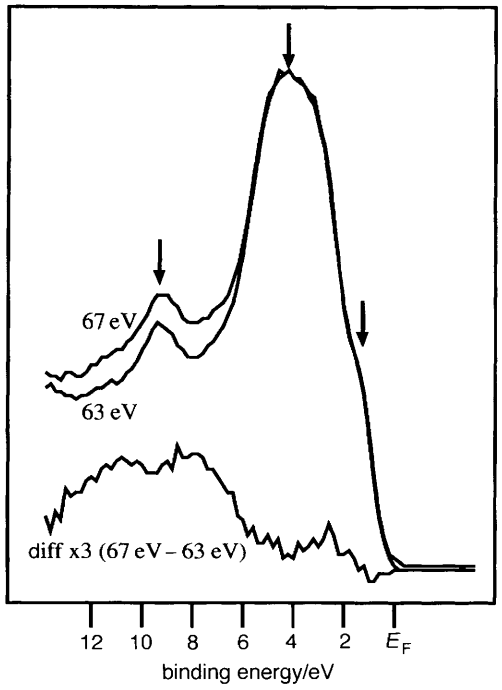

Fig. 3 EDCs showing the valence band and satellite region of a scraped ceramic sample of $La_2NiO_{4+\delta}$, at the Ni 3p → 3d resonance ($h\nu = 67$ eV), off-resonance ($h\nu = 63$ eV) and the difference spectrum, showing the shift in intensity towards the satellite region at resonance. Spectra are normalized to the beam monitor reading. (The binding energy positions marked by arrows refer to the initial state positions used for the CIS measurements shown in Fig. 4.)

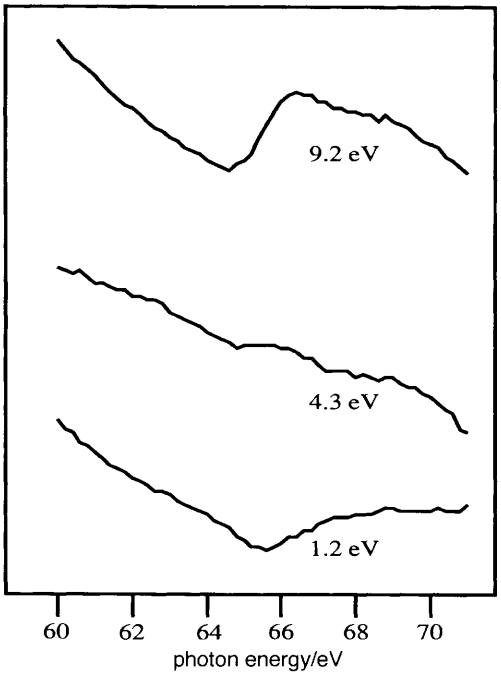

Fig. 4 CIS spectra across the Ni 3p → 3d threshold from scraped ceramic $La_2NiO_{4+\delta}$ at the valence band edge (E_B = 1.2 eV), valence band intensity maximum (E_B = 4.3 eV) and the satellite feature (E_B = 9.2 eV) showing antiresonance at the valence band edge, and resonance at the satellite. (The chosen initial state binding energies are marked by arrows in Fig. 3.) Spectra are normalized to the beam monitor reading. The tungsten absorption coefficient of the beam monitor is featureless in this photon energy range.

Fe-doped samples, and is in good agreement with the data of Eisaki *et al.*[4] for samples with $y = 0$.

The 3p → 3d resonant effects are seen for a wide range of transition metal oxides. The processes occurring are described for a general $3d^n$ initial state configuration below. In this case, the direct photoemission process can be written:

$$3p^6 3d^n + h\nu \rightarrow 3p^6 3d^{n-1} + e^-$$

At photon energies larger than the 3p → 3d adsorption threshold, the direct process is supplemented by initial 3p → 3d excitation, followed by super Coster-Kronig Auger decay:

$$3p^6 3d^n + h\nu \rightarrow \{3p^5 3d^{n+1}\}^* \rightarrow 3p^6 3d^{n-1} + e^-$$

Resonant effects are attributed to interference between direct and indirect channels. Using this model, Ni threshold resonances have been interpreted as implying strong d character in the valence band density of states, as in an unscreened pure $3d^{n-1}$ configuration, whilst anti-resonance (where the dip in the Fano resonance shape is larger than the succeeding maximum) is interpreted as indicating a screened final state of the type $3d^n\underline{L}^1$. The observation of an antiresonance at the p → d threshold for ligand hole final states in the late transition metal oxides is confirmed by cluster calculations such as those of Fujimori and Minami for NiO.[13] The resonant behaviours observed in Fig. 4 thus confirm that the states to the low binding energy side of the main valence band arise mainly from Ni $d^8\underline{L}$ final states, with the satellite feature at around 9.5 eV binding

energy representing the unscreened Ni d^7 configuration. The valence band intensity maximum at around 4 eV binding energy shows no resonant effect, and we attribute it to O 2p states, which are essentially non-bonding for samples that contain no Fe.

Fig. 5 shows corresponding CIS data taken at the Fe $3p \rightarrow 3d$ resonance for an Fe-doped sample, $La_{1.1}Sr_{0.9}Fe_{0.2}Ni_{0.8}O_{4+\delta}$. These data are typical of those taken for all Fe-doped samples, and show some Fe contribution to the DOS for all parts of the valence band and satellite regions. In this respect the data are in good agreement with CIS spectra of simple iron oxides, such as Fe_xO ($x \approx 0.95$), Fe_3O_4 and Fe_2O_3.[14–16] The position of the resonance is of some interest as a guide to the Fe valency in these systems. Whereas the Ni resonance does not appear to shift significantly with change in oxidation state[6] the corresponding shifts in position of the Fe resonance appear to be quite significant.[16] Lad and Henrich[16] note that the onset of the resonance depends on the oxidation state of the Fe cation, and correlates with the Fe 3p binding energies determined by XPS. These authors show CIS data with a resonance maximum at $\approx$ 56.3 eV for Fe^0, $\approx$57.8 eV for Fe^{II} and $\approx$ 58.2 eV for Fe^{III}. In our case, the low amount of Fe dopant incorporated into the samples means that the resonances are rather weak. However, it appears that the resonance maximum is located in the range 58.2–58.6 eV. No resonant data for Fe^{IV} are available for comparison, but we suggest that the resonance position measured is indicative of a high valence state of $\geqslant$3.0 for Fe. The data are thus consistent with the work of Benloucif *et al.*,[2] who conclude that these materials contain predominantly Fe^{III}, but also Fe^{IV} valencies.

The resonances shown in Fig. 5 appear to be slightly stronger in the satellite region (binding energy 12.2 eV) than in the central part of the valence band. Configuration

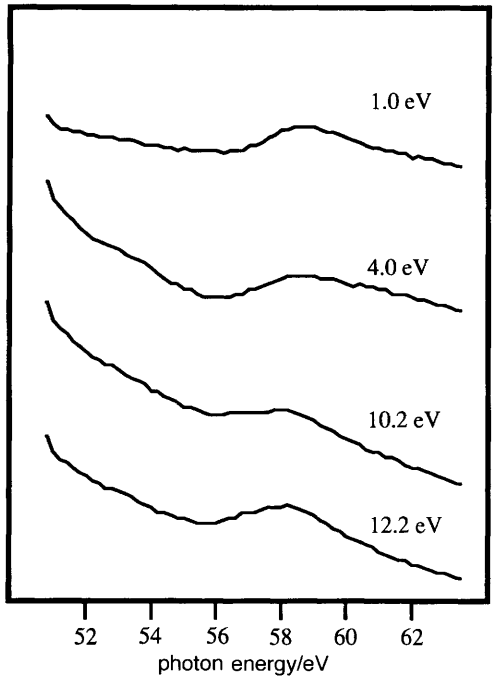

Fig. 5 CIS spectra across the Fe $3p \rightarrow 3d$ threshold from scraped ceramic $La_{1.1}Sr_{0.9}Fe_{0.2}Ni_{0.8}O_{4+\delta}$ at the valence band edge ($E_B = 1.0$ eV), valence band intensity maximum ($E_B = 4.0$ eV) and the satellite region ($E_B = 10.2$, 12.2 eV) showing resonance across the valence band DOS. Spectra are normalized to the beam monitor reading. The tungsten absorption coefficient of the beam monitor is featureless in this photon energy range.

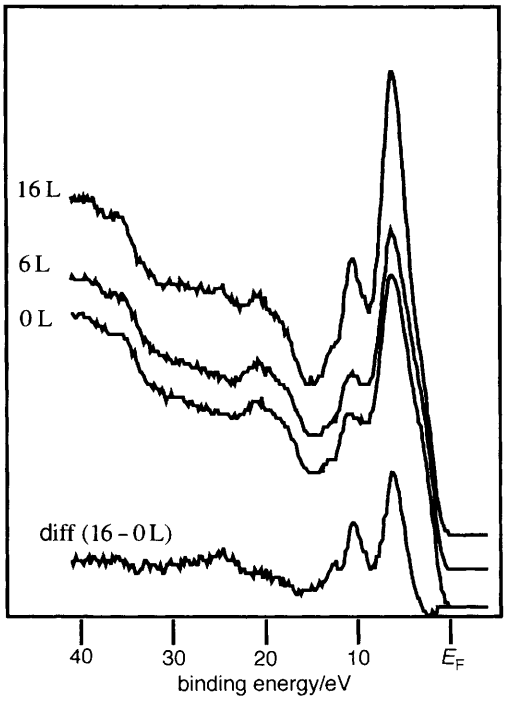

Fig. 6 Photoemission spectra of freshly-scraped and CO-dosed $La_{1.1}Sr_{0.9}Ni_{0.8}Fe_{0.2}O_{4+\delta}$ at 132 K using 95 eV photon energy. The difference spectrum was obtained by normalizing the intensity on the leading valence band edge of the substrate, away from the adsorbate-induced features.

interaction calculations for Fe_2O_3 show that the Fe contribution to the main part of the valence band arises mainly from a screened $d^5\underline{L}^1$ final state, with the satellite region arising from overlapping d^4 and $d^5\underline{L}^1$ contributions, peaking at around 13 eV binding energy.[14,15] We would expect to see quite a strong resonance from the unscreened d^4 contribution, as sampled by our CIS data for 12.2 eV binding energy. Nevertheless, it is clear that there is a substantial contribution to the whole of the main valence band from Fe, with the O 2p states strongly hybridized with Fe throughout, as observed for simple Fe oxides.[14–16] A similar broad valence band contribution is observed for the neighbouring element, Co, in the complex oxide $Bi_2Sr_2CoO_{6+\delta}$.[17] We note that, as in the simple binary Fe oxides,[14–16] the $d^5\underline{L}^1$ states appear to show resonant, rather than anti-resonant behaviour. However, the states sampled at 1 and 4 eV binding energies show a more pronounced dip prior to resonance than the satellite states, with a delayed resonance maximum at 58.6 eV compared with 58.2 eV for the satellite features, which we suggest is indicative of their screened nature.

Thus our resonant photoemission studies indicate that the DOS at the leading edge of the valence band close to E_F has both Fe and Ni character, suggesting that these ions will be readily involved in the catalytic redox process, and is consistent with the ease with which these cations can be oxidized in this material. As Sr is doped into the oxide, this DOS moves closer to E_F, suggesting increasing ease of electron removal from this density of states, *i.e.* increasing stability of high transition metal oxidation states and redox flexibility. The movement of the edge on hole doping appears to be more marked for samples doped with even quite low levels of Fe, suggesting that addition of Fe has quite a strong influence on the redox behaviour of the material, facilitating the Ni^{II}–Ni^{III} redox process. For hypochlorite decomposition using the Hydecat catalyst, this process

is thought to be rate limiting.[3] Thus our experiments reveal an electronic influence of Fe on the DOS close to E_F, which offers a possible rationalization of the rate enhancements observed on adding low levels of Fe to the Hydecat material.

Adsorption studies. Fig. 6 shows the effect of dosing a scraped surface of $La_{1.1}Sr_{0.9}Ni_{0.8}Fe_{0.2}O_{4+\delta}$ with CO at low temperature. Similar results were obtained for other values of x and y, including $x = 0$ and $y = 0$. The figure shows the spectrum obtained from a freshly scraped surface (0 L) and the spectra obtained after successive doses of CO (6 and 16 L). The difference spectrum (16 − 0 L) is also shown. This difference spectrum was characteristic of all the samples, and was retained on warming the samples to room temperature, as shown in Fig. 7. The most obvious changes on dosing are an increase in the intensity of the valence band at around 6 eV, and a striking increase in the intensity of the satellite peak at around 10 eV binding energy. This suggests that at least part of the intensity of this feature on the freshly scraped sample is due to contamination from CO fragments in the residual vacuum, and indeed, this feature is seen to increase in intensity with time after scraping. The difference spectrum

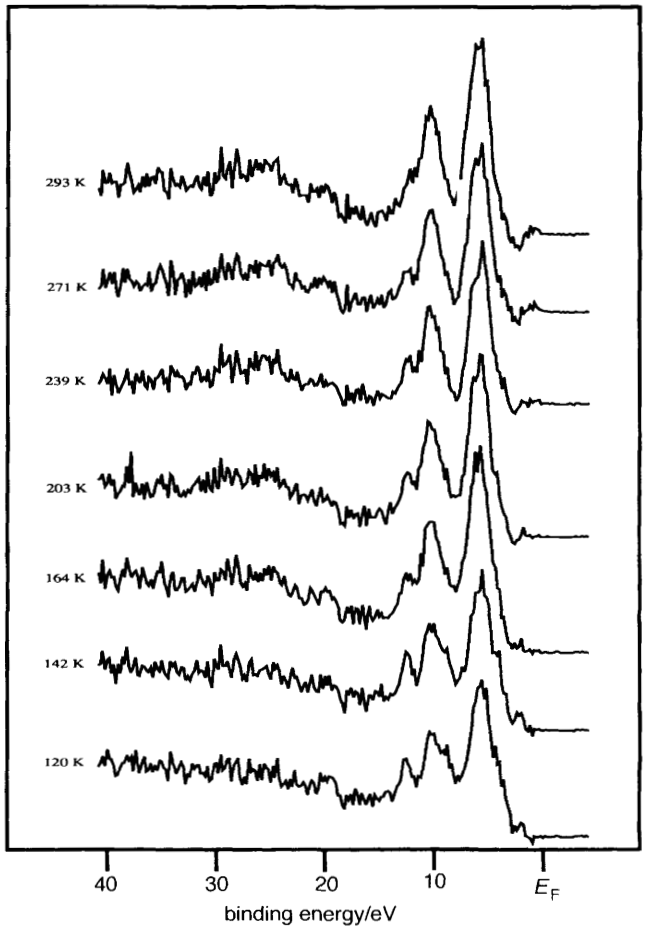

Fig. 7 Difference photoemission spectra (obtained as in Fig. 6, 16–0 L) at 95 eV photon energy for CO-dosed $LaSrNi_{0.8}Fe_{0.2}O_{4+\delta}$ as a function of sample temperature on warming from 120 K.

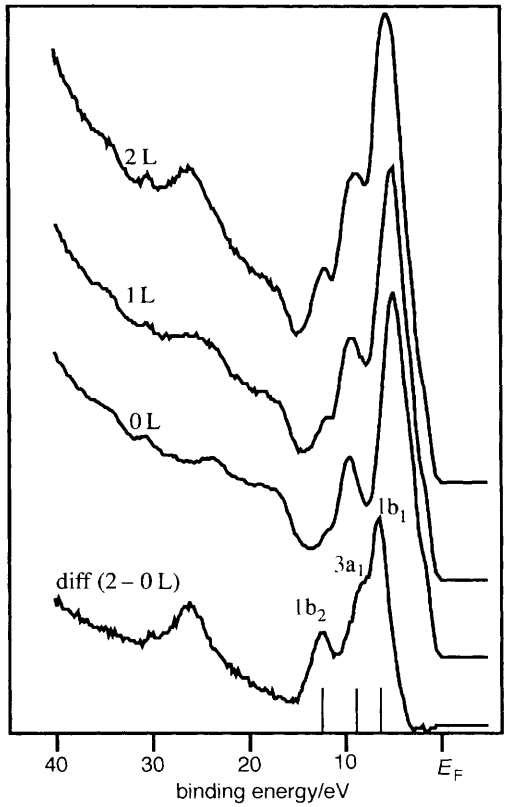

Fig. 8 Photoemission spectra of freshly-scraped and H_2O-dosed $La_2NiO_{4+\delta}$ at 125 K using 75 eV photon energy. The difference spectrum was obtained by normalizing the intensity on the leading valence band edge of the substrate, away from the adsorbate-induced features. Vertical ionization energies for gas-phase water[21] are also shown, aligned at the $^1b_2$ peak positions.

(Fig. 6) reveals the binding energies of the CO-induced features to be 6.2 and 10.4 eV, with a further small peak evident at 12.5 eV. The observation of three new features is strongly suggestive of the oxidation of the CO species to CO_2 or a carbonate species. By comparing the features with the gas-phase photoelectron spectrum of CO_2, one can loosely associate the peak at 6.2 eV with the $1\pi_g$ molecular orbital, the peak at 10.4 eV to the overlapping $1\pi_u$ and $2\sigma_u$ orbitals and the 12.5 eV feature with the $2\sigma_g$ level. However, in common with Kurtz *et al.*[18] we find that the energy separation of the features in the difference spectrum does not exactly accord with those in CO_2, but does give good agreement with the spectra of bulk carbonates such as $CaCO_3$. The energy separations of the features (4.3 and 2.2 eV) are also in excellent agreement with the results of Kurtz *et al.*[18] for CO and CO_2 adsorption on the corresponding cuprate $La_{2-x}Sr_xCuO_4$; the latter shows corresponding separations of 4.4 and 2.2 eV.

Our adsorption spectrum is rigidly shifted by 1.2 eV to higher binding energy relative to that recorded for CO_2 adsorption on the conducting cuprate,[18] compared with a shift of 2 eV to higher binding energy for bulk carbonate. We associate this with the difference in substrate conductivity between the doped nickelate (semiconducting) and the corresponding cuprate (metallic), giving an enhanced final state polarization–relaxation shift for the latter. A similar effect has been observed in water adsorption studies on complex metal oxides of this type.[19]

Our results indicate that $La_{2-x}Sr_xNi_{1-y}Fe_yO_{4+\delta}$, like $La_{2-x}Sr_xCuO_4$, readily oxidizes CO to a carbonate-like surface species, which is strongly bound to the surface, remaining even at room temperature. We note that the electrode potential for the oxidation of CO to CO_2 in aqueous solution is as small as 0.1 eV, indicating that although just spontaneous, the reaction is roughly neutral in thermodynamic terms. The ready formation of carbonate under the present conditions suggests that the oxidizing nature of the nickelate surface is assisting the reaction. Similar behaviour has been observed on NiO(100), where CO is observed to abstract surface O and desorb as CO_2.[20]

As a test of chemical reactivity, the adsorption of CO is quite undiscriminating in this case, as all the surfaces tested produced carbonate, regardless of Sr or Fe doping level. However, some differentiation between different surface reactivities was possible using water as a probe molecule. Fig. 8 and 9 show the results of water dosing La_2NiO_4 (Fig. 8) and $La_{1.1}Sr_{0.9}NiO_4$ (Fig. 9) at low temperature. In Fig. 8, three peaks at binding energies of 6.6, 8.7 and 12.4 eV are evident in the difference spectrum. The appearance of three adsorbate peaks, two of which lie below the valence band of the substrate is typical for non-dissociative adsorption of water on metal oxides.[21] By comparison with data for other oxides,[19] these features can be assigned to the $1b_1$, $3a_1$ and $1b_2$ molecular orbitals of undissociated water, respectively. The peak separations Δ ($3a_1 - 1b_1$) of 2.1 eV and $\Delta(1b_2 - 3a_1)$ of 3.7 eV compare well with those of gas-phase water (2.1 and 3.8 eV, respectively).[22] It is now well established that for strong chemisorption to the surface, the $3a_1$ molecular orbital of the adsorbed water experiences a shift to higher binding energy relative to the other orbitals compared with its position in gas-phase water.[19] The absence of any large shift of this type here suggests that water is not strongly chemisorbed to the surface at low temperature. This result can be contrasted with that

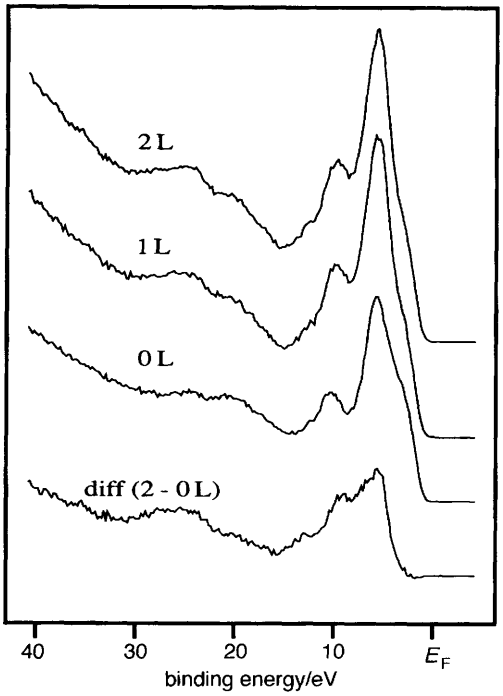

Fig. 9 Photoemission spectra of freshly-scraped and H_2O-dosed $La_{1.1}Sr_{0.9}NiO_{4+\delta}$ at 125 K using 75 eV photon energy. The difference spectrum was obtained by normalizing the intensity on the leading valence band edge of the substrate, away from the adsorbate-induced features.

found for a Sr-doped sample, $La_{1.1}Sr_{0.9}NiO_{4+\delta}$, shown in Fig. 9. A poorer signal-to-noise ratio in these data makes it difficult to locate the peaks in the difference spectrum with certainty, but we estimate them to be at ≈ 5, 8.6 and 11.7 eV, giving $\Delta(3a_1 - 1b_1)$ of ≈ 3.6 eV and $\Delta(1b_2 - 3a_1)$ of ≈ 3.1 eV, *i.e.*, there is a very significant bonding shift of the $3a_1$ molecular orbital to lower binding energy, suggesting strong (but still non-dissociative) adsorption of water to the surface at low temperatures. Both data sets, for $La_2NiO_{4+\delta}$ and for $La_{1.1}Sr_{0.9}NiO_{4+\delta}$ show rather large polarization–relaxation shifts relative to the gas-phase ionization potential of the $1b_1$ level of gas-phase water at 12.6 eV,[22] of 6 eV for $La_2NiO_{4+\delta}$ and 7.6 eV for $La_{1.1}Si_{0.9}NiO_{4+\delta}$. Again we associate the larger shift for the Sr-doped material with the increasing conductivity of the material as Sr is doped into the nickelate.

Fig. 10 shows the typical behaviour of a water-dosed sample on warming past room temperature. At 148 K, the difference spectrum for $LaSrNiO_{4+\delta}$ shows three peaks at binding energies of 5.2, 8.8 and 12 eV, corresponding to the $1b_1$, $3a_1$ and $1b_2$ molecular orbitals of undissociated water (again showing a strong bonding shift of the $3a_1$ molecular orbital for this Sr-doped sample), together with a broad peak in the range 24–25 eV binding energy, corresponding to O 2s emission from the dosed water. At 323 K, the

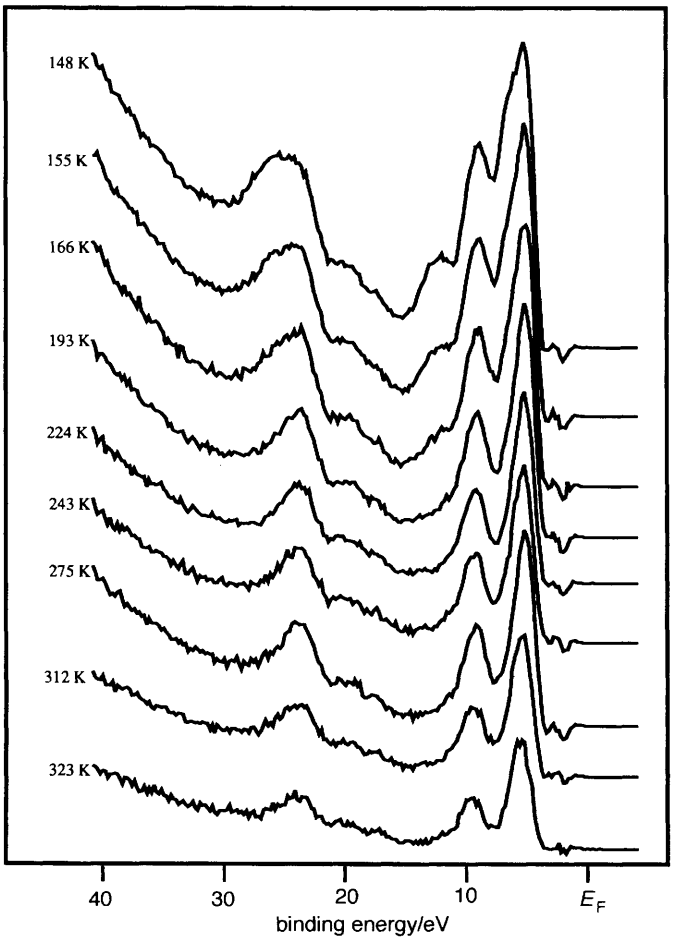

Fig. 10 Difference photoemission spectra (obtained as in Fig. 9, 30–0 L) at 75 eV photon energy for H_2O-dosed $LaSrNiO_{4+\delta}$ as a function of sample temperature on warming from 148 K.

absolute intensity of the last feature has decreased, and in the valence band region, only two features are now observed, at binding energies of 5.5 and 10.3 eV. We associate these features with the 1π and 3σ orbitals of adsorbed OH groups, which appear at 4.9 and 9.0 eV binding energy in the spectra of the corresponding metallic cuprate.[18] Thus, the adsorbed water dissociates as the sample is warmed leaving surface hydroxide, which is not desorbed even at room temperature. The temperature at which dissociation occurs is difficult to estimate from the difference plots, but intensity from the $1b_2$ molecular orbital of water disappears completely between 166 and 193 K. Similar behaviour was observed for other Sr-doped compositions, although cross-contamination from CO adsorption precludes a full comparison of the dissociation temperature for all samples. However, we note that Fe doping appears to have little effect on the temperature at which water dissociates, and we measure the complete disappearance of the $1b_2$ signal at a temperature between 169 and 193 K for $La_{1.1}Sr_{0.9}Ni_{0.8}Fe_{0.2}O_{4+\delta}$. A change in the Sr content appears to have a more marked effect, with the corresponding temperature range for $La_{1.3}Sr_{0.7}Ni_{0.8}Fe_{0.2}O_{4+\delta}$ found to be 189–202 K. On the undoped material $La_2NiO_{4+\delta}$, a rather different result was obtained, with the difference spectrum being almost completely lost by 163 K, suggesting that water desorbed from this surface at low temperature without dissociating. These observations imply that the surfaces become more reactive to water as the Sr content increases, with dissociation of water being promoted by Sr doping. This is consistent both with stronger chemisorption of water at low temperature on Sr-doped samples, and also with the empirical observation that the samples become increasingly unstable to degradation as the Sr content is increased. Thus we conclude that although Fe doping appears to have little effect on the initial adsorption and dissociation of H_2O, the samples appear to become increasingly reactive to water as the Sr concentration increases.

High resolution ESCA studies

With the last observation in mind, high resolution XPS of the as-presented samples was carried out. The aim was to quantify the surface Sr concentration and to study its effect on the reactivity of the samples to atmospheric gases, and their long term degradation. Complex oxides of this type typically react with air containing H_2O and CO_2, forming degradation products (often carbonates or hydroxides) at the surface. These reactions have been most closely studied in recent years for the superconducting cuprates, where atmospheric degradation poses significant technological problems.[23–25] The effects of atmospheric degradation on the XPS spectra of the cuprates have been established in some detail.[24,25] These include the appearance of a C 1s feature due to carbonate, and high binding energy shoulders on several of the main peaks, including the alkaline earth metal signals and O 1s. These features have been attributed to the formation of degradation products at the surface, including hydroxides and alkaline-earth carbonate.[24,25] In view of the close relationship between the nickelate and superconducting cuprates, we can reasonably expect to observe some similar behaviour here.

Fig. 11 shows the Al-Kα XPS spectra recorded in the O 1s region for samples of $La_{2-x}Sr_xNiO_{4+\delta}$ having varying Sr contents. A double peaked structure reminiscent of that found in the cuprates is observed for all compositions. The high binding energy signal rises in intensity with time spent in the vacuum, is enhanced in grazing emission, and is reduced when the surface is scraped in UHV using a diamond file. These features strongly suggest that this signal is associated with surface degradation. For $La_2NiO_{4+\delta}$, the high binding energy feature is of relatively low intensity, and is of a width comparable with the main signal. We attribute the low binding energy signal to oxygen in the bulk nickelate, and the higher binding energy peak to surface degradation products; in common with $La_2CuO_{4+\delta}$ and La_2O_3, it seems likely that this signal is due to surface hydroxide species when $x = 0$. For the Sr-doped samples, a much broader signal of

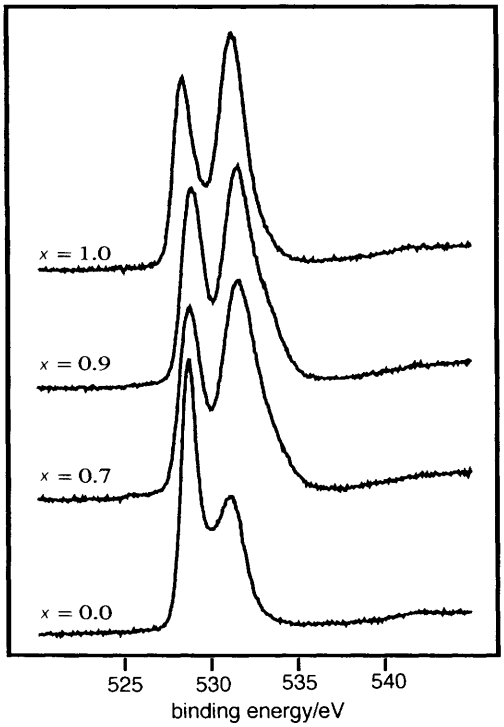

Fig. 11 Normal emission Al-Kα XPS of the O ls region for samples in the series $La_{2-x}Sr_xNiO_{4+\delta}$

higher intensity is observed. It is clear that several components are present here, and any fit to the data would be speculative. However, we note that the corresponding Sr 3p features show high binding energy shoulders, and that a peak due to CO_3^{2-} is now observed in the C 1s region. We suggest that as well as surface hydroxide, the degradation products now include $SrCO_3$. The formation of the alkaline-earth carbonate is catalysed in the presence of atmospheric water vapour by initial formation of the hydroxide, which then reacts with CO_2 to form the carbonate.[25] These results suggest that the surface reactivity to degradation increases with Sr doping, and is consistent with our studies of the effects of water dosing under controlled conditions.

The surface Sr/La ratio is of some interest, as Sr clearly affects surface reactivity. Quite marked segregation of Sr has been observed previously for related perovskites, such as $La_{1-x}Sr_xVO_3$ [26] and $La_{1-x}Sr_xCoO_3$,[27] and for layered perovskites, such as $La_{2-x}Sr_xCuO_4$.[28] Fig. 12 shows a comparison of the data from the present study with these literature measurements. The ratios for the nickelate samples have been obtained by integration of the Sr signal from the bulk nickelate alone, *i.e.*, the high binding energy part of the Sr signal, due to second phases formed by surface degradation, has not been included. This has the result that the diagram emphasizes the intrinsic surface segregation of Sr within the nickelate phase, and the data can be compared directly with results from the literature where surface contaminant phases have been removed. It can be seen that marked intrinsic segregation is observed in the nickelate phase, and more remarkably, that it follows essentially the same variation with bulk doping level as in other related oxides. This is apparently driven because the ionic radius of the Sr^{2+} dopant is larger than that of the host La^{3+}. The dopant produces less elastic strain when accommodated at the surface rather than at bulk sites. An enhanced concentration of Sr is therefore available at the surface of these materials, which, as our results show, enhances

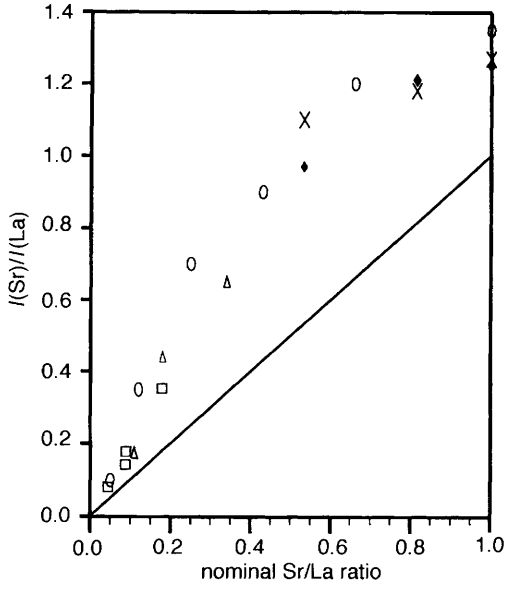

Fig. 12 The XPS Sr/La intensity ratio (corrected for ionization cross-sections) plotted against nominal bulk Sr/La ratio for perovskite and layered perovskite materials. ○, $La_{1-x}Sr_xVO_3$;[26] △, $La_{1-x}Sr_xCoO_3$;[27] □, $La_{2-x}Sr_xCuO_4$,[28] × and ◆ represent data for $La_{2-x}Sr_xNiO_{4+\delta}$ and $La_{2-x}Sr_xFe_yNi_{1-y}O_{4+\delta}$, respectively (this work), calculated using the Sr signal intensities from the nickelate phases alone. The line shows the ratio expected in the absence of surface Sr segregation.

the reactivity of the surface to subsequent reaction, *e.g.*, with the atmosphere to form carbonates.

Conclusions

The valence band electronic structure of $La_{2-x}Sr_xNi_{1-y}Fe_yO_{4+\delta}$ has been explored for $x = 0$–1.1 and $y = 0$–0.2. The effect of Sr (hole) doping is seen by a shift of the leading valence band edge towards E_F on doping. However, metallic behaviour (in terms of a clear Fermi cut-off at E_F) is not observed over this range of x, consistent with stronger electron–phonon coupling in this material than in the related superconducting cuprate.[12]

The resonant behaviour at the transition metal 3p → 3d thresholds reveals that the leading edge of the valence band has both Fe and Ni character, leading us to suppose that this part of the DOS profile is comprised of strongly hybridized Fe/Ni 3d–O 2p states. This is consistent with the ease of oxidation of the transition metal ions in this material. The edge movement towards E_F on Sr doping is consistent with increased ease of oxidation and redox flexibility on hole doping. This edge movement appears to be significantly affected by doping with relatively low levels of Fe, suggesting that Fe influences the ease of the Ni^{II}–Ni^{III} redox process. As this is thought to be rate-limiting for hypochlorite decomposition over the related Hydecat catalyst, this suggests a possible reason for the strong influence of low-level Fe-doping on the activity of this material.

Adsorption measurements show that all the surfaces are sufficiently oxidizing to produce carbonate-like species from CO readily. However, some discrimination in surface reactivity is obtained in water dosing experiments. Water is chemisorbed more strongly and dissociates at lower temperatures on Sr-doped samples than on undoped

samples. This suggests that the surface reactivity to water increases with Sr concentration. High resolution ESCA studies of as-presented samples reveal that Sr is segregated to the surface of these oxides, and that the segregation behaviour is consistent with that seen in related oxides including $La_{2-x}Sr_xCuO_4$. The Sr-doped samples show marked surface degradation, to products probably including surface hydroxide and $SrCO_3$. As for superconducting cuprates, the production of carbonate can be catalysed by initial hydroxide formation, which is strongly favoured on the Sr-doped materials.

The nature of the initial adsorption site is of some interest. In a ceramic sample, many different sites will be available. Assuming that, as for La_2CuO_4, the predominant exposed face is (001), then either La(Sr)–O or Ni–O_2 planes could be exposed at the surface. The increasing reactivity to water with Sr doping could simply be associated with adsorption at an increasing number of Sr surface sites in La(Sr)–O surface planes. However, the Sr doping also modifies the electronic structure at the Ni sites, and this could affect their reactivity. Recent work has shown that the expected octahedral site for Ni^{2+} in $La_2NiO_{4+\delta}$ is slightly Jahn–Teller distorted (presumably due to the presence of some Ni^{3+}), with a gap of around 1.3 eV between the O 2p/$3d_{z^2}$ and O 2p/$3d_{x^2-y^2}$ upper Hubbard bands.[12] For a coordinatively unsaturated surface Ni site (roughly square pyramidal), this distortion can be expected to be enlarged. Ni^{2+} had a d^8 configuration, with one unpaired electron in each of these bands. On Sr doping, the Ni site is oxidized, leading to depopulation of the upper $d_{x^2-y^2}$ band, but (for the doping levels studied here) no significant change in population of the d_{z^2} band. In cases of strong chemisorption, the interaction between water and transition metal cations on oxide surfaces is of a donor–acceptor type, with, for example, direct donation from the filled $3a_1$ orbital of water, into any empty metal 3d levels of the correct symmetry (in this case $3d_{z^2}$). This leads to a bonding stabilization of the donor levels, and an antibonding destabilization of the acceptor metal d level.[29] This model would lead us to suppose that oxidation of Ni^{2+} to Ni^{3+} *via* Sr doping would not necessarily have a strong influence on the strength of chemisorption at the Ni site as the population of the d_{z^2} acceptor level is unaffected by the doping. In addition, as the d_{z^2} level is partially occupied, we would expect to see the antibonding shift of this level in a shift to lower binding energy of the filled d DOS in the upper part of the valence band on chemisorption, which is not observed here. Thus, we cannot infer bonding of water to the transition metal site from the results presented here, and a single crystal surface structural measurement, *e.g.*, by SEXAFS, will be necessary to distinguish the adsorption site.

This work was funded by EPSRC and ICI Katalco. We thank B. Beagley and J. Spindura for assistance in interpreting the XRD measurements.

References

1 W. R. Flavell, J. Hollingworth, J. F. Howlett, A. G. Thomas, Md. M. Sarker, S. Squire, Z. Hashim, M. Mian, P. L. Wincott, D. Teehan, S. Downes and F. E. Hancock, *J. Synchrotron. Radiat.*, 1995, **2**, 264.
2 R. Benloucif, N. Nguyen, J. M. Greneche and B. Raveau, *J. Phys. Chem. Sol.*, 1991, **52**, 381.
3 E. King and E. E. Hancock, *Catal. Today*, 1996, **27**, 203.
4 H. Eisaki, S. Uchida, T. Mizokawa, H. Namatame, A. Fujimori, J. van Elp, P. Kuiper, G. A. Sawatzky, S. Hosoya and H. Katayama-Yoshida, *Phys. Rev. B*, 1992, **45**, 12513.
5 V. I. Anisimov, M. A. Korotin and E. Z. Kurmaev, *J. Phys.: Condens. Matter*, 1990, **2**, 3987.
6 M. R. Thuler, R. L. Benbow and Z. Hurych, *Phys. Rev. B*, 1983, **27**, 2082.
7 M. A. van Veenendaal, G. A. Sawatzky and W. A. Groen, *Phys. Rev. B*, 1994, **49**, 1407.
8 A. Fujimori, *J. Phys. Chem. Solids*, 1992, **53**, 1595.
9 A. Chainani, M. Mathew and D. D. Sarma, *Phys. Rev. B*, 1992, **46**, 9976.
10 H. Takagi, T. Ido, S. Ishibashi, M. Uota, S. Uchida and Y. Tokura, *Phys. Rev. B*, 1989, **40**, 2254.
11 M. James and J. P. Attfield, *J. Mater. Chem.*, 1996, **6**, 57.
12 E. Pellegrin, J. Zaanen, H-J. Lin, G. Meigs, C. T. Chen, G. H. Ho, H. Eisaki and S. Uchida, *Phys. Rev. B*, 1996, **53**, 10667.
13 A. Fujimori and F. Minami, *Phys. Rev. B*, 1984, **30**, 957.

14 A. Fujimori, N. Kimizuka, M. Taniguchi and S. Suga, *Phys. Rev. B*, 1987, **36**, 6691.
15 A. Fujimori, M. Saeki, N. Kimizuka, M. Taniguchi and S. Suga, *Phys. Rev. B*, 1986, **34**, 7318.
16 R. J. Lad and V. E. Henrich, *Phys. Rev. B*, 1989, **39**, 13478.
17 H. Eisaki, H. Takagi, S. Uchida, H. Matsubara, S. Suga, M. Nakamura, K. Yamaguchi, A. Misu, H. Namatame and A. Fujimori, *Phys. Rev. B*, 1990, **41**, 7188.
18 R. I. Kurtz, R. Stockbauer, T. E. Madey, D. Mueller, A. Shih and L. Toth, *Phys. Rev. B*, 1988, **37**, 7936.
19 W. R. Flavell, J. H. Laverty, D. S-I. Law, R. Linsay, C. A. Muryn, C. F. J. Flipse, G. N. Raiker, P. L. Wincott and G. Thornton, *Phys. Rev. B*, 1990, **41**, 11623.
20 J. M. McKay and V. E. Henrich, *J. Vac. Sci. Technol. A*, 1987, **5**, 722.
21 S. Eriksen, P. D. Naylor and R. G. Egdell, *Spectrochim. Acta, Part A*, 1987, **43**, 1535.
22 K. Siegbahn, *J. Electron Spectrosc. Relat. Phenom.*, 1974, **5**, 1.
23 A. Barkatt, H. Hojaji, V. R. W. Amarakoon and J. G. Fagan, *MRS Bull.*, 1993, **18**, 45.
24 M. S. Golden, R. G. Egdell and W. R. Flavell, *J. Mater. Chem.*, 1991, **1**, 489 and references therein.
25 W. R. Flavell, D. R. C. Hoad, A. J. Roberts, R. G. Egdell, I. W. Fletcher and G. Beamson, *J. Alloys Compounds*, 1993, **195**, 535 and references therein.
26 R. G. Egdell, M. R. Harrison, M. D. Hill, L. Porte and G. Wall, *J. Phys. C: Solid State Phys.*, 1984, **17**, 2889.
27 J. P. Kemp, D. J. Beal and P. A. Cox, *J. Solid State Chem.*, 1990, **86**, 50.
28 R. G. Egdell, W. R. Flavell and M. S. Golden, *Supercond. Sci. Technol.*, 1990, **3**, 8.
29 See, for example, V. E. Henrich and P. A. Cox, *The Surface Science of Metal Oxides*, Cambridge University Press, Cambridge, 1994, p. 258.

Paper 6/05278I; *Received* 29*th July*, 1996